Supporting Information for

North China Plain as a hot spot of ozone pollution exacerbated by extreme high temperatures

Pinya Wang[1], Yang Yang[1*], Huimin Li[1], Lei Chen[1], Ruijun Dang[2], Daokai Xue[3], Baojie Li[1], Jianping Tang[3], L. Ruby Leung[4], Hong Liao[1]

[1]Jiangsu Key Laboratory of Atmospheric Environment Monitoring and Pollution Control, Jiangsu Collaborative Innovation Center of Atmospheric Environment and Equipment Technology, School of Environmental Science and Engineering, Nanjing University of Information Science and Technology, Nanjing, Jiangsu, China

[2]School of Engineering and Applied Science, Harvard University, Cambridge, MA, USA

[3]School of Atmospheric Sciences, Nanjing University, Nanjing, Jiangsu, China

[4]Atmospheric Sciences and Global Change Division, Pacific Northwest National Laboratory, Richland, Washington, USA

Correspondence to: Y. Yang, yang.yang@nuist.edu.cn

Contents of this file

Text S1 to S2

Figures S1 to S8

Table S1 to S2

Text S1

Evaluation of OPCs simulated by GEOS-Chem during 2014-2017.

The GEOS-Chem simulated OPCs/OPIs during May-September 2014-2017 are identified using the same method described in Section 2 of the main text for observations. The spatial patterns of OPC and CF values of 2014-2017 are illustrated in Figure S5. The simulated OPC and CF spatial patterns are comparable to those of the observations, with higher values over the NCP region (37-41^{o}N; 114 -120^{o}E). The spatial correlation between the simulated and observed OPCs is higher than 0.5. The regional mean OPCs and CF values over NCP in observations are 19 days and 30%, respectively, while those in the GEOS-Chem simulation are 22 days and 35%. The model can reasonably reproduce the observed spatial patterns of OPCs and CF values and their magnitudes over NCP during 2014-2017.

Text S2

Evaluation of OPCs in the CMIP6 simulations of present climate.

Here, the CMIP6 simulated OPCs are again identified using the same method described in Section 2. The spatial patterns of OPC and CF during 2015-2019 in observation and CMIP6 simulations under four SSPs are illustrated in Figure S6. The simulated OPCs and CF show similar spatial patterns compared to the observations, with higher values over the NCP regions (Figure S6). The regional mean OPC and CF over NCP (37-41^{o}N; 114 -120^{o}E) in the observations are 28 days and 37% respectively, during 2015-2019. The multi-model ensemble mean of CMIP6 simulations can reasonably reproduce the magnitudes of OPCs and CF values over NCP, with highest values under SSP2-4.5 (34 days & 44.5%) and lowest values under SSP3-7.0 (20.3 days &26.5%).

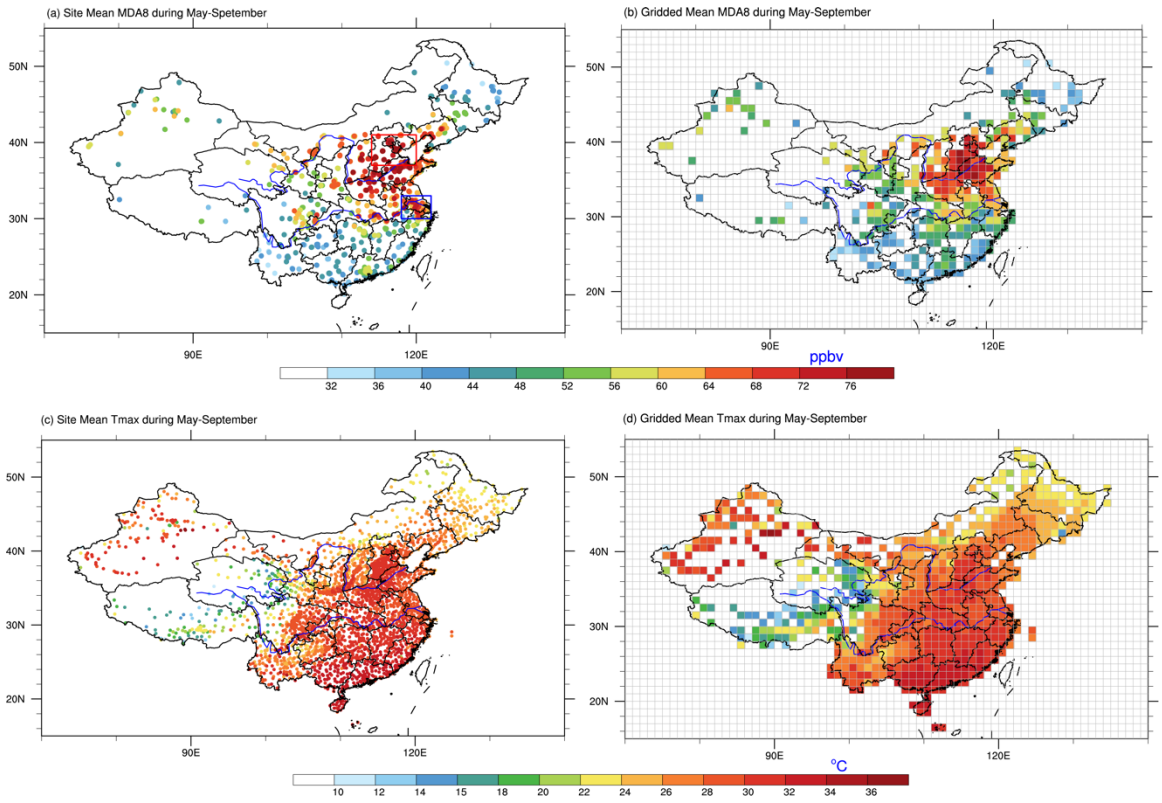

Figure S1. Spatial distributions of (a) site mean and (b) gridded mean MDA8 O_3, and (c) site mean and (d) gridded mean Tmax during May-September for 2014-2019. The red box and blue box in panel (a) represent the NCP region (37-41ºN; 114-120ºE) and the YRD region (30-33ºN; 118-120ºE), respectively.

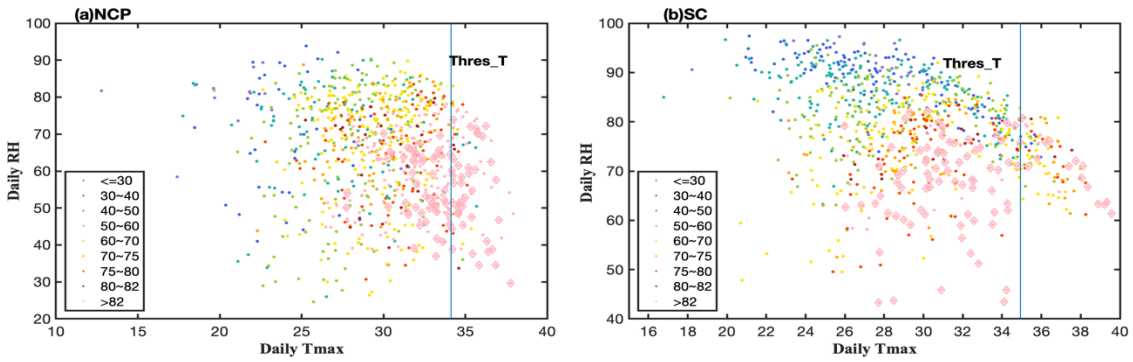

Figure S2. Daily MDA8 O_3 (ppbv, colored dots) as a function of the local daily Tmax and RH during May-September of 2014-2019 over (a) NCP (37-41°N; 114-120°E) and (b) YRD (30-33°N; 118-122°E). The larger pink squares denote the ozone pollution days with daily MDA8 O_3 exceeding the O_3 threshold. The vertical blue line denotes the threshold for extreme Tmax (Thres_T). Thus, the larger pink squares on the right side of the blue line represent coupled extreme days OPCs.

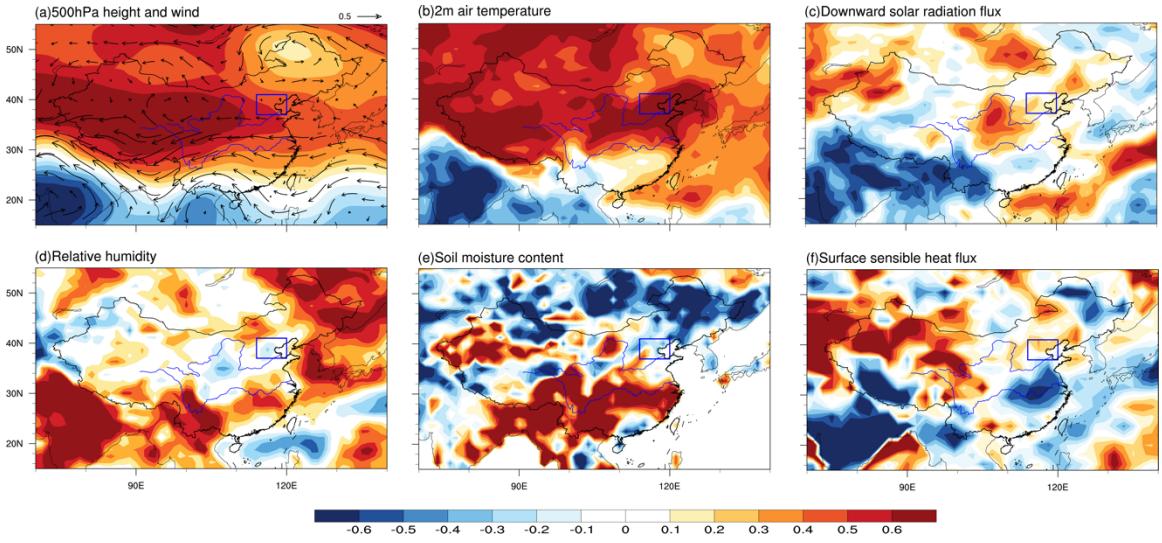

Figure S3. Differences between OPCs and OPIs (OPCs minus OPIs) composites of normalized anomalous (a) geopotential height and winds at 500hPa, (b) 2m air temperature, (c) downward solar radiation flux (DSR), (d) relative humidity, (e) soil moisture content, and (f) surface sensible heat flux. The blue box in each panel indicates the NCP region (37-41°N; 114-120°E).

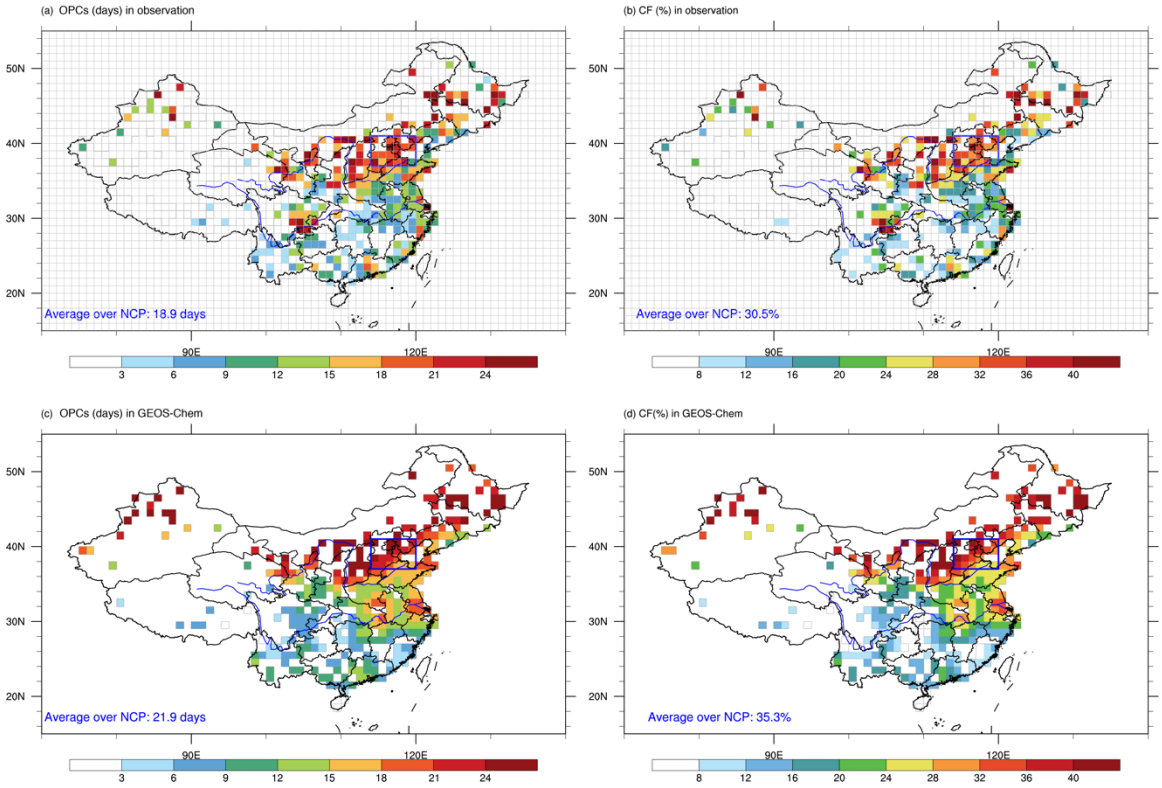

Figure S4. Spatial patterns of observed (a) OPCs (days) and (b) CF values (%) during May-September of 2014-2017. (c) and (d) are same as (a) and (b) but for the GEOS-Chem simulation. Observed and simulated values of OPCs(days) and CF averaged over NCP (37-41°N; 114-120°E) are indicated at the bottom left corner of each panel.

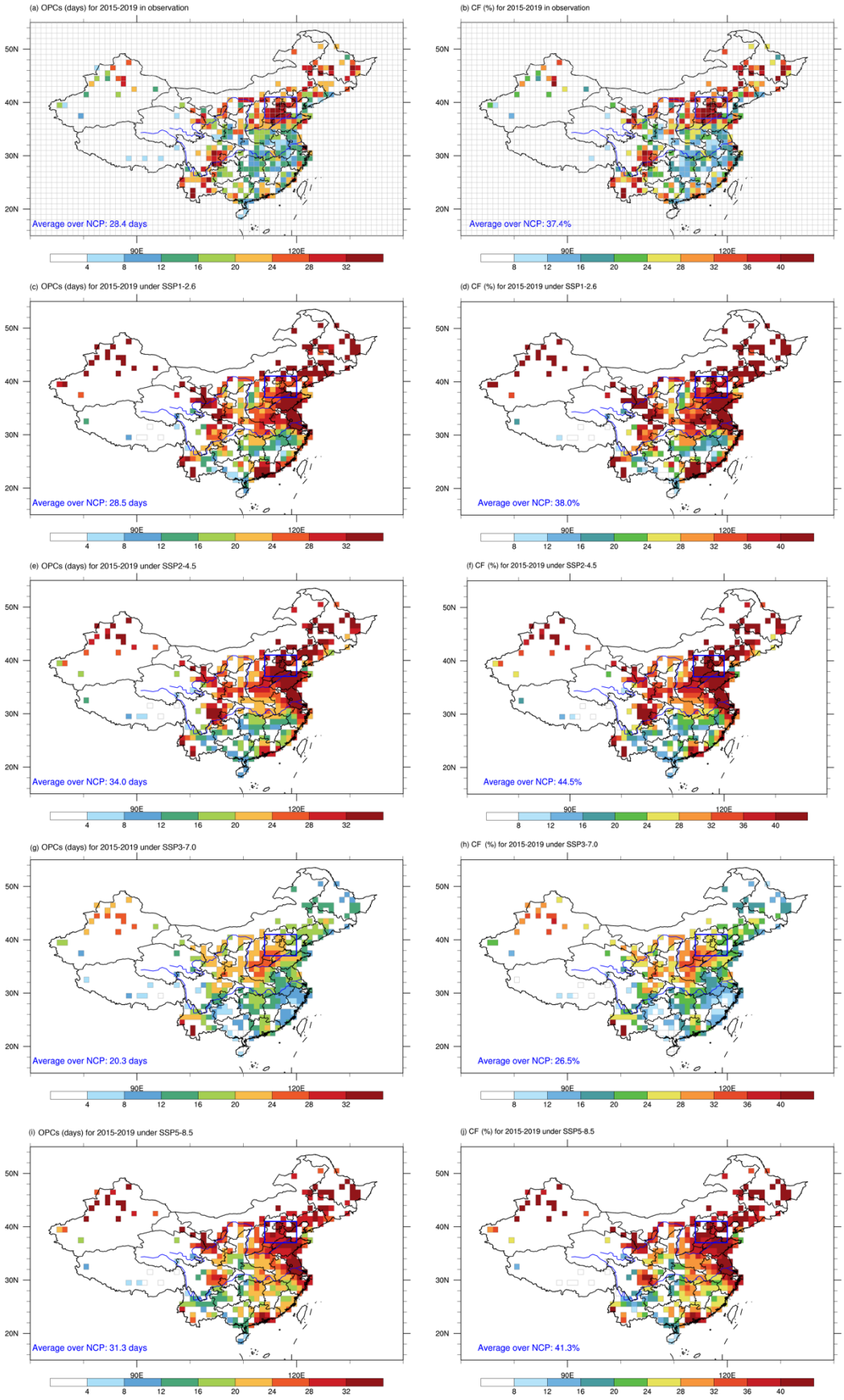
(a) OPCs (days) for 2015-2019 in observation
Average over NCP: 28.4 days
(b) CF (%) for 2015-2019 in observation
Average over NCP: 37.4%
(c) OPCs (days) for 2015-2019 under SSP1-2.6
Average over NCP: 28.5 days
(d) CF (%) for 2015-2019 under SSP1-2.6
Average over NCP: 38.0%
(e) OPCs (days) for 2015-2019 under SSP2-4.5
Average over NCP: 34.0 days
(f) CF (%) for 2015-2019 under SSP2-4.5
Average over NCP: 44.5%
(g) OPCs (days) for 2015-2019 under SSP3-7.0
Average over NCP: 20.3 days
(h) CF (%) for 2015-2019 under SSP3-7.0
Average over NCP: 26.5%
(i) OPCs (days) for 2015-2019 under SSP5-8.5
Average over NCP: 31.3 days
(j) CF (%) for 2015-2019 under SSP5-8.5
Average over NCP: 41.3%
50N
40N
30N
20N
90E
120E
4 8 12 16 20 24 28 32
8 12 16 20 24 28 32 36 40

Figure S5. Spatial patterns of (a) OPCs (days) and (b) CF values (%) during May-September of 2015-2019 in observation; (c)~(d), (e)~(f), (g)~(h), and (g)~(h) are same as (a) and (b) but for CMIP6 simulations under SSP1-2.6, SSP2-4.5, SSP3-7.0 and SSP5-8.5, respectively. OPCs (days) and CF averaged over NCP (37-41°N; 114-120°E) are indicated at the bottom left corner of each panel.

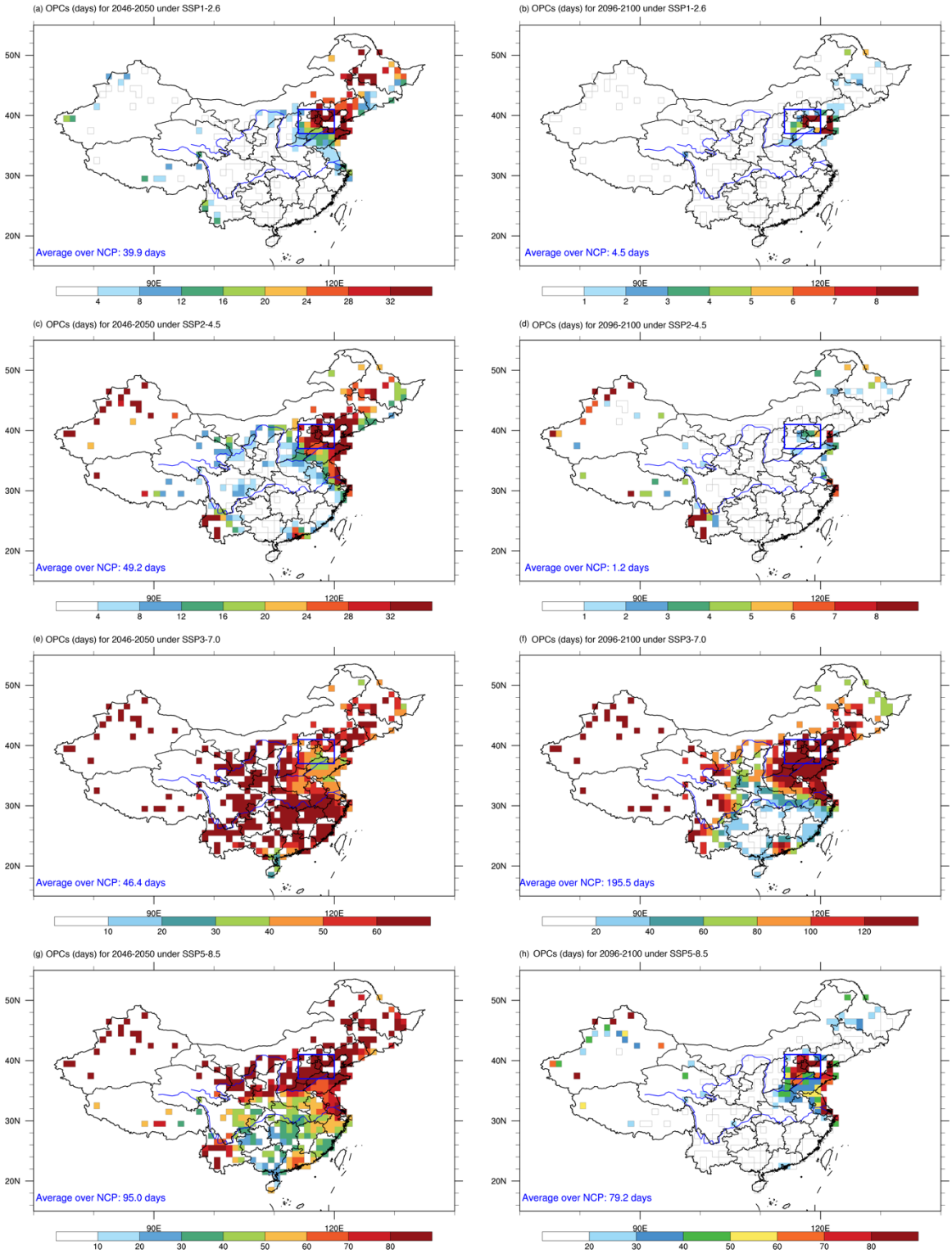

Figure S6. Spatial patterns of OPCs (days) during May-September in (a) 2046-2050 and (b) 2096-2100 under SSP1-2.6; (c)~(d), (e)~(f) and (g)~(h) are same as (a)~(b) but for simulations under

SSP2-4.5, SSP3-7.0 and SSP5-8.5, respectively. OPCs averaged over NCP (37-41ºN; 114-120ºE) are indicated at the bottom left corner of each panel.

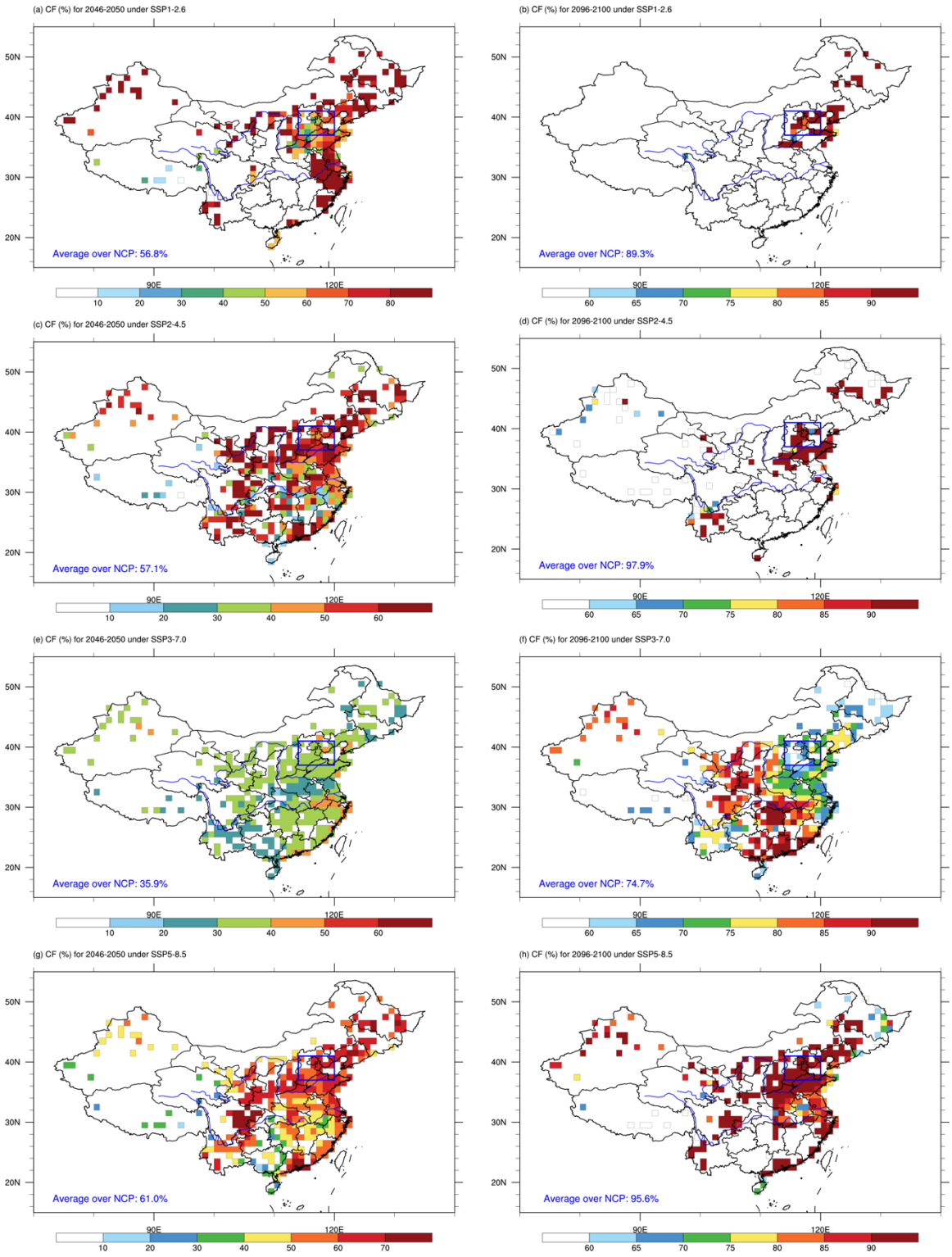

Figure S7. Same as Figure S6, but for CF values (%). CF values (%) averaged over NCP (37-41°N; 114-120°E) are indicated at the bottom left corner of each panel.

Figure S8. Changes in annual mean (a) Tmax and (b) MDA8 O_3 averaged over NCP (37-41°N; 114-120°E) relative to 2015 under SSP1-2.6, SSP2-4.5, SSP3-7.0 and SSP5-8.5. The colored lines indicate the multi-model ensemble mean for each SSP and the scattered dots with the same color denote results across the available CMIP6 models. The three periods of 2015 to 2019, 2046 to 2050 and 2096 to 2100 are marked with gray shading.

Table S1. Information of the CMIP6 models used in this study.

Model	Horizontal Resolution (Lon x Lat)	Time range	Institution
MOHC.UKESM1-0-LL	192 x 144	2015-2100	MOHC
CESM2-WACCM	288x 144	2015-2100	NCAR
GFDL-ESM4	288x180	2015-2100	NOAA-GFDL
MPI-ESM-1-2-HAM	192x96	2015-2055	HAMMOZ-Consortium
EC-Earth3-AerChem	120x90 for O_3 concentration 512x256 for temperature	2015-2100	EC-Earth-Consortium

Table S2 Models (ticked) providing simulations for each SSP scenario. Note that most of the adopted models provide hourly O_3 concentration and daily Tmax except the MOHC.UKESM1-0-LL simulations under SSP5-8.5 provide 3-hourly surface air temperature (Tas) and the GFDL-ESM4 simulations under SSP2-4.5 provide hourly Tas; thus, daily Tmax for the two GCMs are derived from hourly or 3-hourly Tas.

Model	SSP1-2.6	SSP2-4.5	SSP3-7.0	SSP5-8.5	Citation
MOHC.UKESM1-0-LL	√	√	√	√	Good et al. (2019)
CESM2-WACCM		√		√	Danabasoglu G (2019)
GFDL-ESM4		√			John et al. (2018)
MPI-ESM-1-2-HAM			√		Neubauer et al., 2019
EC-Earth3-AerChem			√		EC-Earth Consortium (EC-Earth) (2019)

131

132 References

133 Consortium, E. C.-E. (2019). EC-Earth-Consortium EC-Earth3-Veg model output prepared for
134 CMIP6 ScenarioMIP, Earth System Grid Federation.
135 Danabasoglu, G. (2019). NCAR CESM2-WACCM model output prepared for CMIP6
136 ScenarioMIP, Earth System Grid Federation.
137 Good, P., et al. (2019). MOHC UKESM1.0-LL model output prepared for CMIP6 ScenarioMIP,
138 Earth System Grid Federation.
139 John, J. G., et al. (2018). NOAA-GFDL GFDL-ESM4 model output prepared for CMIP6
140 ScenarioMIP, Earth System Grid Federation.
141 Neubauer, D., et al. (2019). HAMMOZ-Consortium MPI-ESM1.2-HAM model output prepared
142 for CMIP6 AerChemMIP, doi:10.22033/ESGF/CMIP6.1621, 2019.